Journal of Science and Transport Technology
Journal homepage: https://jstt.vn/index.php/en

Vehicle Classification Using Combined Laser Rangefinder and Pyroelectric Infrared Sensors in a Real Dynamic Environment

Vu Van Quang[2], Nguyen Van Tuan[2], Nguyen Nam Anh[2], Nguyen Tien Dung[2], Vu Toan Thang[2], Bui Hai Dang[1,2,*]

[1]Faculty of Information Technology, University of Transport Technology, No 54 Trieu Khuc Street, Thanh Liet Ward, Hanoi 100000, Vietnam

[2]Precision Engineering & Smart Measurements Lab, School of Mechanical Engineering; Hanoi University of Science and Technology, No 1 Dai Co Viet Street, Bach Mai Ward, Hanoi 100000, Vietnam

Article info
Type of article:
Original research paper

DOI:
https://doi.org/10.58845/jstt.utt.2026.en.6.1.111-122

***Corresponding author:**
Email address:
dangbh@utt.edu.vn

Received: 14/04/2025
Received in Revised Form: 20/11/2025
Accepted: 06/12/2025

Abstract: This paper presents a vehicle classification approach for real-world dynamic environments based on sensor fusion between a laser rangefinder (LRF) and a pyroelectric infrared (PIR) sensor. By integrating geometric shape information from the LRF with thermal distribution patterns captured by the PIR sensor, the system extracts distinctive features that effectively suppress noise introduced by external environmental variations. A lightweight neural network is developed for classification, achieving a minimum accuracy of 91% for specific vehicle types and an average accuracy of 94% across all categories. Owing to its high accuracy and low computational cost, the proposed model is well-suited for implementation in portable embedded platforms, functioning as intelligent measurement nodes within Intelligent Transportation Systems (ITS).

Keywords: Vehicle classification, Laser Rangefinder, Pyroelectric Infrared, neural network, dynamic environments.

1. Introduction

Vehicle detection and classification are essential components in the development of Intelligent Transportation Systems (ITS), enabling critical functions such as traffic flow regulation, speed monitoring, incident detection, and electronic toll collection [1–3]. As urbanization accelerates globally, the demand for real-time traffic analysis and smart infrastructure continues to rise, particularly in densely populated metropolitan areas [4].

A variety of sensor technologies have been employed to address vehicle classification tasks. Among these, vision-based systems—including closed-circuit television (CCTV) cameras, and thermal imaging—are widely adopted due to their ability to capture rich spatial and appearance information. However, these systems exhibit significant drawbacks in practical deployments. They require a high-cost equipment, substantial computational resources, and are sensitive to environmental disturbances such as poor lighting, occlusions, and adverse weather conditions [5]. Although vision systems enhanced by deep learning techniques, such as convolutional neural networks (CNNs), have demonstrated high accuracy in ideal conditions, and traditional image-based feature extraction methods such as histogram of oriented gradients (HOG), scale-invariant feature transform (SIFT), and speeded-up

robust features (SURF) offer computational efficiency, both approaches struggle to maintain robustness and real-time performance in dynamic and resource-constrained environments [6].

In addition to vision-based approaches, several studies have investigated the use of non-vision-based sensors for vehicle detection and classification. These technologies are often more robust to environmental changes and offer advantages in terms of cost, energy efficiency, and ease of integration in embedded systems. For instance, magnetometers detect variations in the Earth's magnetic field caused by passing vehicles and have demonstrated reliable performance in the real traffic scenarios. However, their deployment requires intrusive installation beneath road surfaces, leading to high costs and complex maintenance [7]. Pyroelectric infrared (PIR) sensors, by contrast, are passive, low-cost, and capable of detecting motion through changes in infrared radiation. Due to their simplicity and low power consumption, they are well-suited for distributed sensing in wireless ITS nodes. However, PIR sensors alone cannot distinguish between different vehicle types, as they lack the capacity to capture structural or shape information [8] Likewise, laser-based ranging sensors, such as laser rangefinders (LRFs) and Light Detection and Ranging (LIDAR) systems, provide accurate geometric information by measuring the distance from the sensor to the vehicle surface. LIDAR generates detailed 3D spatial profiles, while LRF typically yields one-dimensional contour information. Both sensor types can support vehicle shape reconstruction, yet when applied independently, they often fall short in distinguishing between similarly shaped vehicles and typically demand significant computational resources [9,10]

Despite the availability of diverse sensing and classification methods, there remains a gap in systems that are simultaneously accurate, computationally efficient, and suitable for deployment on embedded platforms in dynamic environments. Additionally, while multimodal sensor fusion has been explored to improve robustness, many of these solutions increase system complexity and cost, rendering them unsuitable for widespread deployment in real-world ITS applications [11].

In this study, we address these challenges by proposing a hybrid sensor fusion framework that combines a laser rangefinder with a pyroelectric infrared sensor to leverage their complementary strengths. The LRF provides structural information through distance profiling, while the PIR sensor captures the thermal distribution along a vehicle's body as it moves through the sensing zone. By synchronizing and processing these signals, we extract novel composite features that reflect both the geometric and thermal characteristics of vehicles. These features are used to train a lightweight convolutional neural network, optimized for real-time inference on embedded devices. Compared to traditional feature-based techniques [9-10] and deep vision models [8], our method offers improved robustness, higher classification accuracy, and significantly lower computational cost.

2. Sensor Data Acquisition System and Feature Extraction

2.1. Sensor setup and data acquisition

In this study, a sensor fusion system combining a Laser Rangefinder (LRF) and a Pyroelectric Infrared (PIR) sensor is deployed at roadside and designed to simultaneously capture both distance measurements and thermal radiation patterns as vehicles pass through the sensing field (Fig. 1). By integrating the complementary information from these two sensing modalities, the system aims to improve classification accuracy under varying environmental conditions. Fig. 2 provides a clear vision of the optical system structure applied.

The LRF operates based on the Time-of-Flight (ToF) principle, where it emits laser pulses and measures the time it takes for the signal to return, calculating the distance to an object. This allows the sensor to scan and construct the

vehicle's outline, providing important information about its shape and size, helping distinguish between motorcycles, cars, trucks, and other vehicle types. The system uses the Garmin LIDAR-Lite v3HP, a high-performance laser sensor with a measurement range of 5 cm to 40 m, a resolution of ± 2.5 cm, a sampling rate of 100 Hz, and a scanning angle of 27° [12]. With a high scanning speed, the LRF can track and analyse multiple vehicles at the same time, even when the object moving at high-speed.

In parallel, the PIR module detects the infrared radiation emitted by vehicles. The system utilizes a dual-element PIR sensor with code IRA-S200ST01A01 [13], which operates within the 5 ÷ 14 μm wavelength range. To enhance sensitivity and expand the detection area, a KUBE TR1007 Fresnel lens is integrated in front of the PIR sensor [14]. The multi-segment optical design of the lens focuses infrared radiation from multiple directions onto the sensor, improving angular resolution and detection robustness.

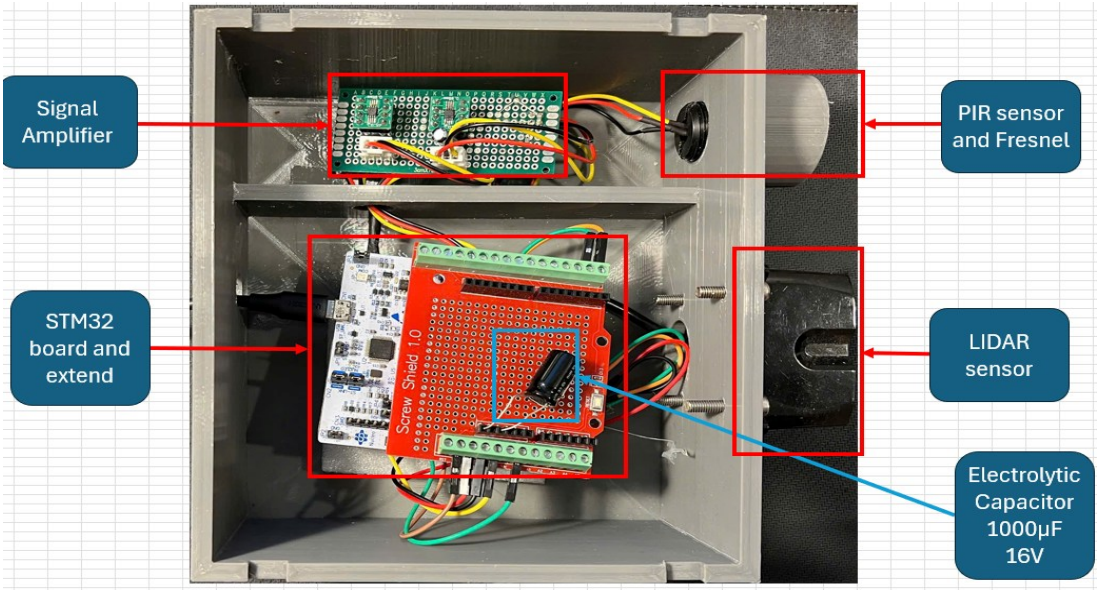

Fig. 1. Image of sensor fusion system

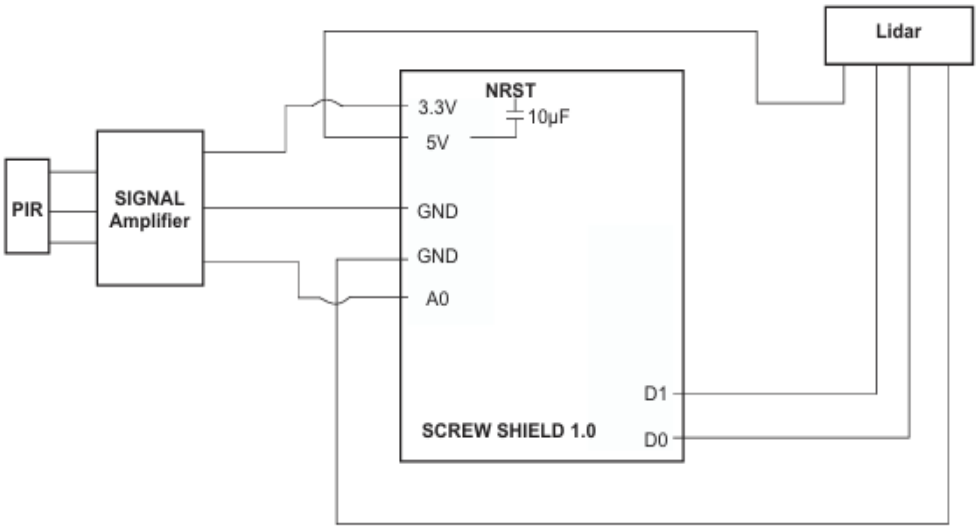

Fig. 2. Schematic diagram circuit diagram

A custom data acquisition board based on an STM32 microcontroller is used to interface with both the LRF and PIR sensors. The Garmin LIDAR-Lite v3HP communicates via I2C, while the analog output from the IRA-S200ST01A01 PIR sensor is digitized using the 12-bit internal ADC. Sensor data

are sampled at 100 Hz, with synchronized acquisition achieved through a timer-based interrupt routine. All measurements are timestamped and transmitted to a host computer via USB (virtual COM port) for offline processing. The system is compact, low-power, and suitable for real-time roadside deployment.

The experimental setup (Fig. 3) consists of both sensors mounted at fixed positions on the roadside, at a horizontal distance L = 0.5 m from the nearest edge of the road surface. The installation heights, h_L of the LRF and h_P of PIR, range from 1.0 m to 1.4 m, allowing the system to effectively cover the vehicle profile from multiple angles. This configuration enables simultaneous acquisition of thermal and geometric data for each passing vehicle, forming the basis for subsequent feature extraction and classification.

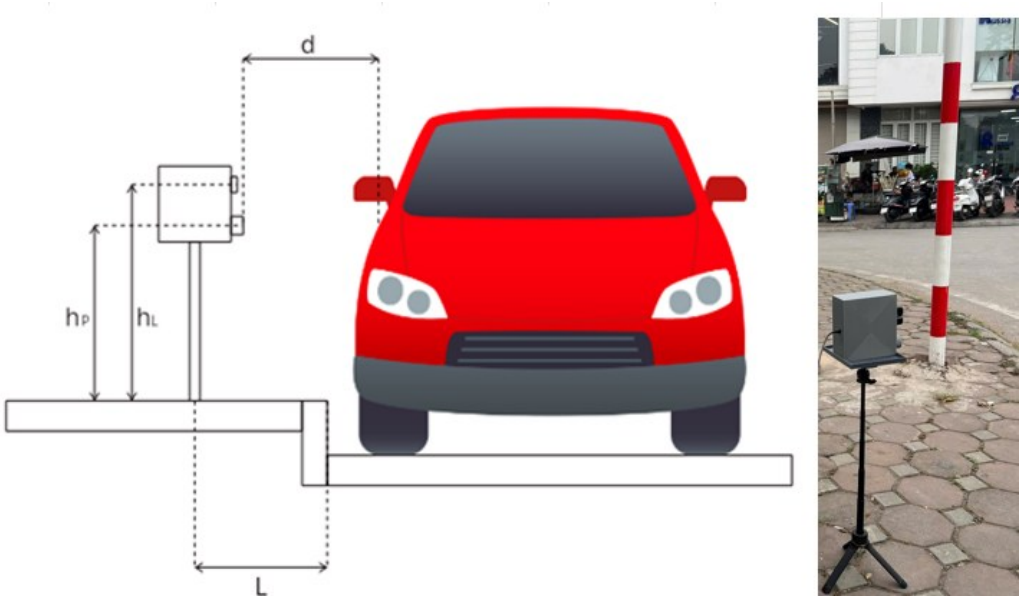

Fig. 3. Schematic diagram of sensor installation geometry (left); and real implementation (right)

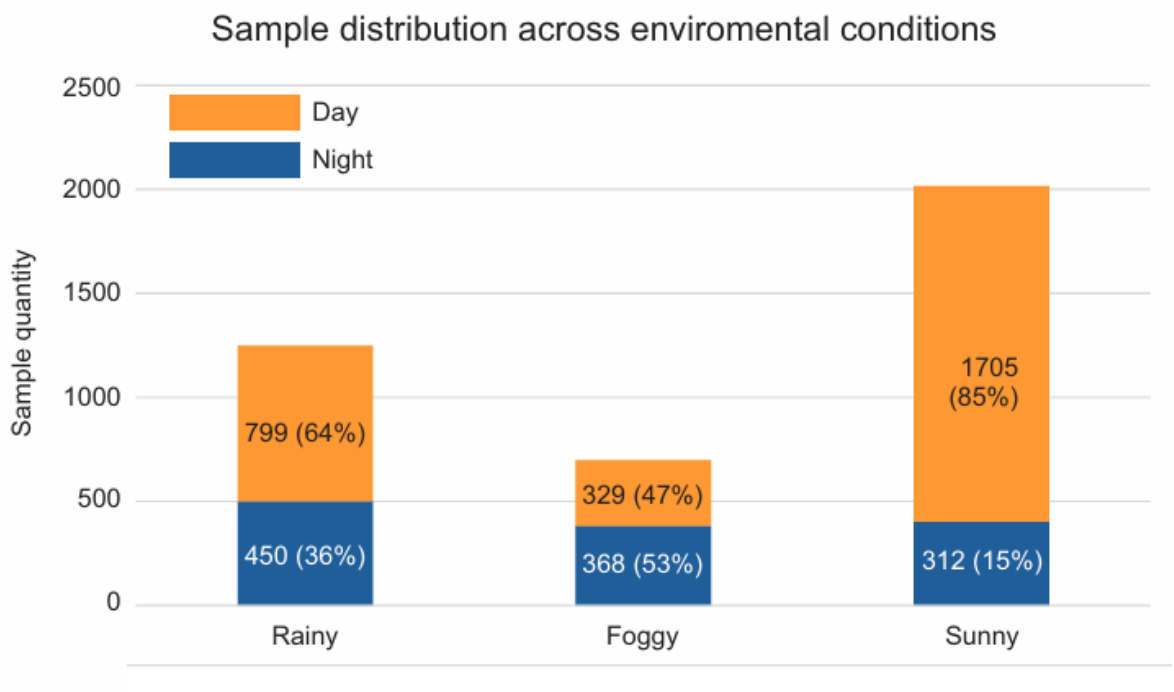

Fig. 4. Sample distribution across environmental conditions

The experimental system was deployed in Hanoi, a city with high traffic density and diverse vehicle types moving at the same time. The experiment was conducted during three different

time periods: morning, afternoon, and evening, all during rush hours. Each experiment session lasted 2 hours, ensuring that the system collected data under various lighting conditions to assess classification stability. The data was collected in different conditions, including day and night, various vehicle speeds in urban and highway environments, and different weather conditions such as clear skies, rain, and fog. During the experiment, a total of 3,963 data samples were collected from different types of vehicles under various environmental conditions (rain, fog, day, night, etc...) as shown in Fig. 4.

2.2. Feature Extraction

The sensor fusion system generates two synchronized signals: the LRF signal, representing the geometric contour of the vehicle, and the PIR signal, reflecting the thermal distribution along the vehicle body. As shown in Fig. 5, the LRF signal (red curve) captures distance variations as vehicles move through the sensing field, while the PIR signal (blue curve) records changes in emitted infrared radiation.

Analysis of the raw signals reveals that larger vehicles such as trucks and buses exhibit stronger amplitude variations in the LRF data, due to their longer and more complex contours. Correspondingly, their PIR signals tend to be stronger, as wider surfaces absorb and emit more thermal energy. In contrast, motorcycles produce relatively smaller fluctuations in both LRF and PIR signals, attributed to their compact structure and lower thermal emission. However, because vehicles such as cars and trucks share similar engine placements (typically at the front), signal peaks may appear in comparable positions, potentially leading to classification ambiguities.

To construct a robust feature set for classification, main components are extracted from the fused data:

- Vehicle contour shape from the LRF signal, and
- Thermal distribution profile from the PIR signal.

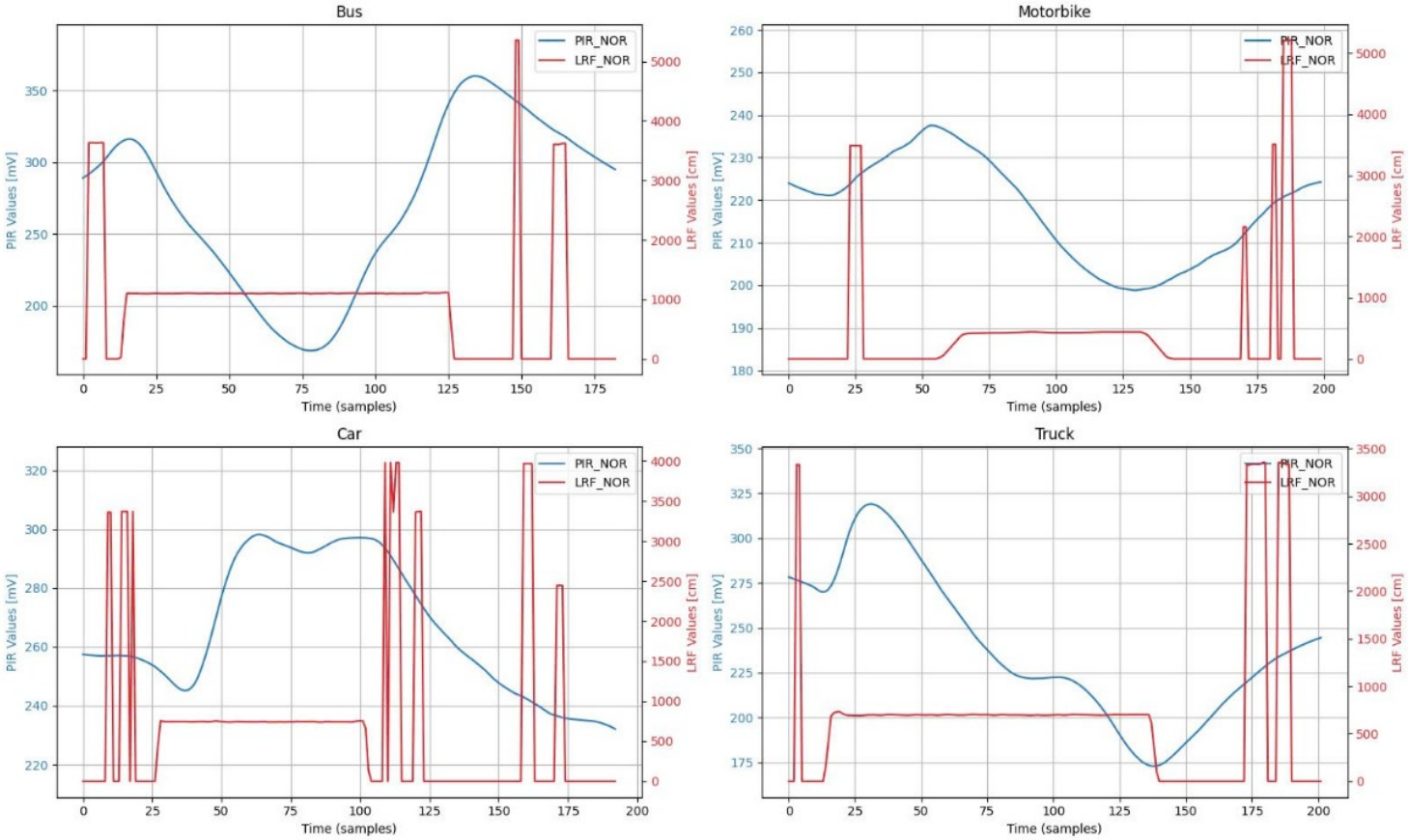

Fig. 5. Raw LRF and PIR sensor signals collected from four representative vehicle types

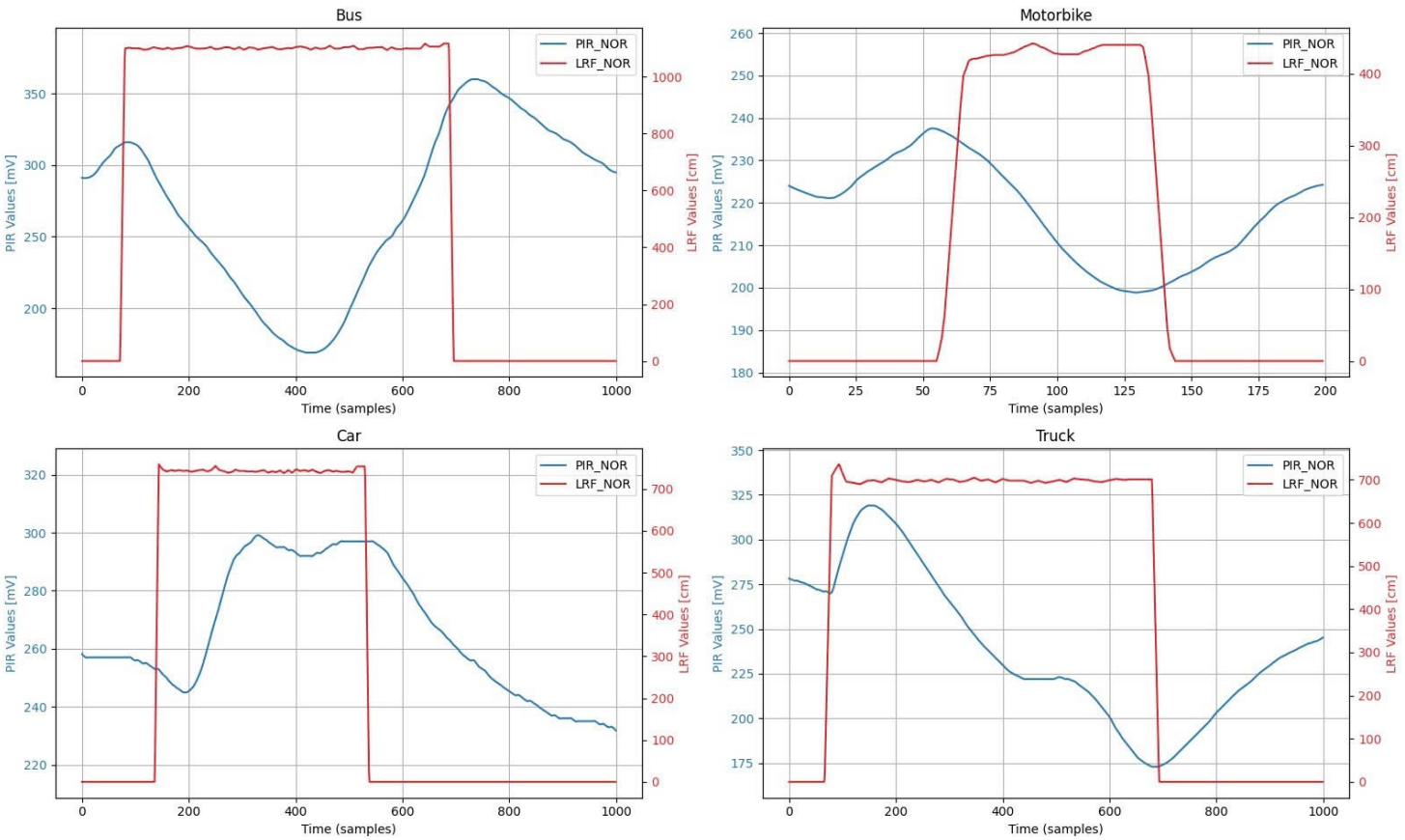

Fig. 6. Normalized LRF and PIR signals representing geometric and thermal profiles of different vehicle types

A key challenge is the variation in vehicle speed, which results in inconsistent numbers of samples per vehicle across data sequences. To address this, the raw sensor data is rescaled to a fixed length of 1000 samples, ensuring uniformity regardless of speed. The input matrix originally includes five data channels—four from the PIR sensors and one from the LRF—which are merged and interpolated using linear interpolation to form a two-column matrix with 1,000 rows (PIR and LRF combined features).

Subsequently, the interpolated signals are rounded to reduce noise, and each feature channel is normalized to the range [0, 1] using min-max scaling. This normalization enhances model generalization and reduces the impact of environmental variability. The resulting signal sequence effectively encodes the thermal distribution along the geometric profile of each vehicle, forming a consistent and discriminative input representation for the deep learning model. Fig. 6 illustrates sample normalized signals for different vehicle types, highlighting the combined shape–thermal signatures that aid the model in learning and classification.

3. Classification Model and Evaluation Results

3.1. Neural Network for Classification

In this study, a Feedforward Neural Network (FNN), specifically a Multilayer Perceptron (MLP), is utilized. FNN is a suitable choice as the input data is structured in tabular form rather than spatial (such as images for CNNs) or sequential (such as time-series data for RNNs). MLP effectively works with the nonlinear relationships between PIR and LRF signals for vehicle classification.

Our model employs two hidden layers, with the number of hidden nodes determined using a formula:

$$\text{Hidden nodes} = \frac{\text{NumberSample}}{\alpha \times (\text{NumberInput} + \text{NumberOuput})} \quad (1)$$

α is within the range (1,2) [15]. Experimental results

using k-fold cross-validation shown that two hidden layers achieve high accuracy while maintaining computational efficiency. A single hidden layer may not be sufficient to learn complex nonlinear relationships between PIR, LRF signals, and vehicle labels, while more than two layers could increase training time without significant accuracy improvement. Optimizing α to prevent overfitting results in an optimal setting of Hidden Nodes [16], and in this study α = 2. Two activation functions are used in the hidden layers are ReLU and Sigmoid. ReLU (equation 2) mitigates the gradient loss problem, enabling faster and more stable learning [17]. It retains positive values while suppressing negative ones, optimizing signal propagation speed.

$$f(x)=\max(0,x) \quad (2)$$

Sigmoid (equation 3) is chosen for the second hidden layer as it limits output values to the range (0,1), making it easier to interpret results as probabilities.

$$\sigma(x)=\frac{1}{1+e^{-x}} \quad (3)$$

The fact is that consecutive Sigmoid layers can cause loss of gradients, reducing model learning efficiency. To balance, ReLU is applied in the first layer to accelerate learning and avoid gradient issues, while Sigmoid in the second layer constrains output values.

The output layer employs the Softmax activation function:

$$S(xi)=\frac{e^{xi}}{\sum_j e^{xj}} \quad (4)$$

With x_i represents the input value of the Softmax function for output class. Softmax ensures that all output values stay within (0,1) and that their sum equals 1, allowing the model to select the class with the highest probability. Unlike Sigmoid which applies independently to each node, SoftMax generates a probability distribution overall output class, improved classification accuracy [18].

Vehicle labels (e.g., motorcycle, car, bus, truck) are encoded using One-Hot Encoding to prevent misunderstand of label order in numerical form.

With this approach, the system achieves high classification accuracy, it can overcome the weaknesses of traditional vision-based methods such as even in low light conditions or complex environments. The model has been tested under various scenarios to ensure stability and generalization. This study proposes an effective approach for vehicle classification using combined PIR and LRF sensor data with deep learning, improving accuracy in challenging conditions.

The input of the model is a matrix with a size of 1,000 rows × 2 columns, corresponding to each vehicle passing through the sensors, resulting in 2,000 input nodes. Since the collected data varies in length depending on vehicle speed, linear interpolation has been applied to standardize the number of collected samples. The data is then normalized to the range [0,1] using scale normalization to ensure stable performance. Vehicle labels are encoded using One-Hot Encoding to prevent the model from class disorder. The neural network has been designed by two hidden layers to balance learning speed and prevent overfitting, the first hidden layer has 32 nodes with ReLU activation, which retains positive values and eliminates negative ones, enabling faster learning and avoiding the vanishing gradient problem. And the second hidden layer has 16 nodes with Sigmoid activation, which normalizes outputs within the probability range (0,1). ReLU is used first before Sigmoid ensures non-linear learning in the first layer before adjusting values into a probability form in the second layer. The final is output Layer, Softmax activation is used to ensure that the sum of output probabilities equals 1. This enhances prediction accuracy and allows confidence comparison between vehicle types. The model is trained on real-world data, where vehicles move at different speeds, including four types: Bus, Car, Truck, and Motorbike. The dataset consists of 3,972 samples, split into a 6-2-2 ratio: Training set: 63% (2,500 samples), Validation set: 20% (800 samples), Testing set: 17% (672

samples).

Since this is a multi-class classification problem, Cross-Entropy Loss is used:

$$L = -\sum_{i=1}^{C} y_i \log \hat{y}_i \quad (5)$$

With C is the number of output classes (four vehicle types), y_i is the actual label, and $\hat{y}_i$ is the predicted probability.

To optimize weights, the Adam Optimizer has been applied, combining Momentum and RMS Prop methods to accelerate convergence and prevent excessively large or small weight updates [19].

3.2. Performance Evaluation

The learning rate is adjusted by parameter search, with an optimal value of 0.0355, as identified in Fig. 7, ensuring stable convergence without excessive fluctuations in weight updates.

Additionally, to prevent overfitting, regularization techniques have been applied. Dropout, a randomly deactivates certain neurons during training to reduce over-reliance on specific features. Weight Decay smooths weight values, preventing excessive growth and mitigating overfitting. By integrating learning rate tuning and regularization methods, the model achieves optimal performance during training while maintaining generalization when deployed on real-world data. The training process is monitored via loss and accuracy values on the validation set. As shown in Fig. 8, the accuracy increases rapidly during the first 20 epochs and stabilizes at 0.93, proving that the model has good learning capability without overfitting. At the same time, Training Loss and Validation Loss significantly decrease and remain low (approximately 0.1), indicating efficient learning and high stability.

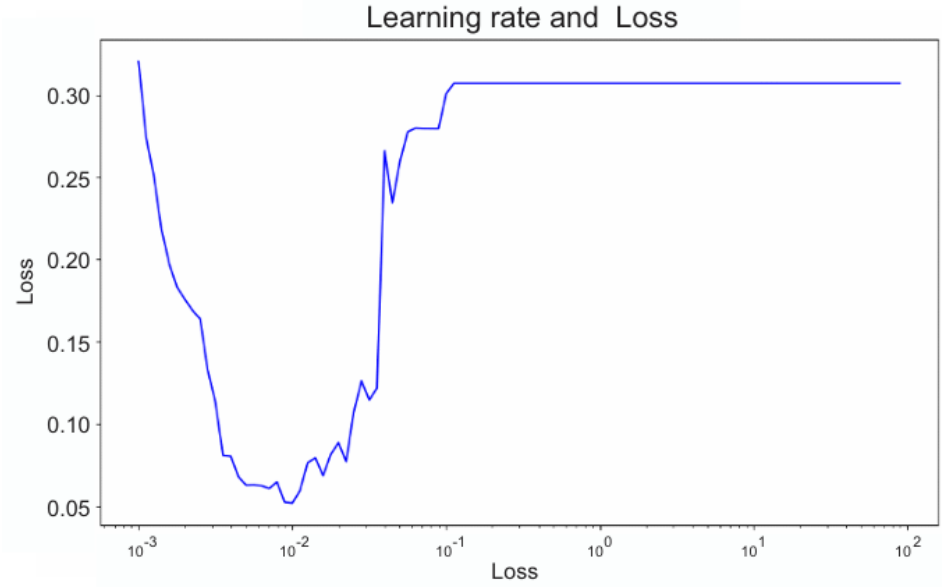

Fig. 7. Learning Rate and Loss

The graph in Fig. 9 visualizes the classification capability across different vehicle types. The vertical axis shows the vehicle type whereas horizontal axis describes the predicted results. Measuring scale with color is also added to support visualizing the amount of each input and output pair. The results indicate that the Bus category achieved 100% accuracy, confirming that the model effectively recognizes the distinct characteristics of this vehicle type, such as its elongated geometric profile in LRF data and broad thermal emission in PIR signals. The Motorbike category also exhibited high accuracy; however, there was an 8.6% misclassification rate with Car, 1.5% with Truck, and 1% with Bus. This misclassification arises primarily from similarities in sensor signatures: Motorbikes and Cars often produce compact LRF contours with comparable peak distances due to similar frontal profiles, while PIR thermal peaks overlap because both emit

concentrated heat from small engines. Similarly, Trucks and Cars share mid-range LRF amplitudes from their boxy shapes, and ambient interference in PIR (e.g., engine heat diffusion in fog) exacerbates ambiguity at detection ranges beyond 1 m, as illustrated in the normalized signals of Fig. 6. The Motorbike and Truck categories experienced higher misclassification rates, mainly being mistaken with Cars, due to these shared thermal and geometric traits under variable speeds. Addressing this could involve speed-normalized filtering to sharpen signal edges.

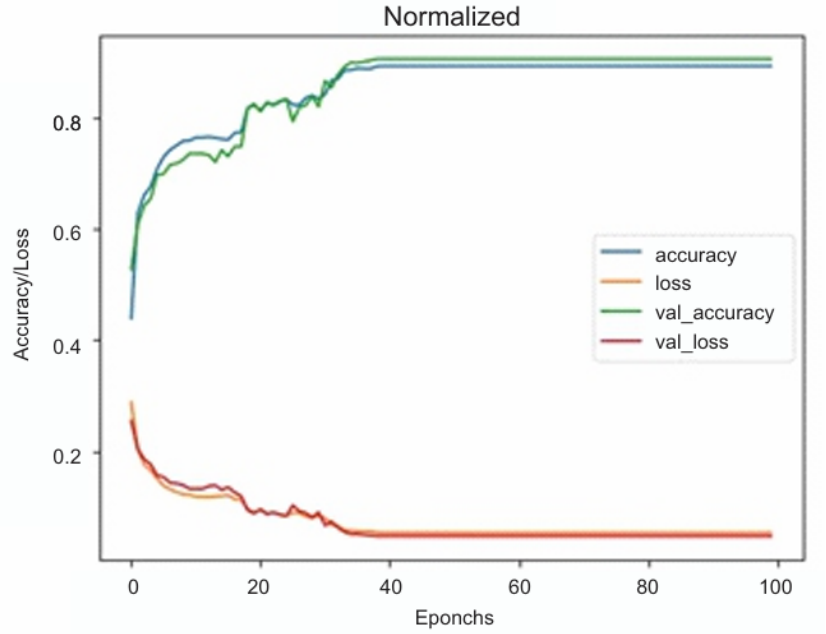

Fig. 8. Performance metrics over epochs of the model trained and tested on PIR sensor and Lidar sensor

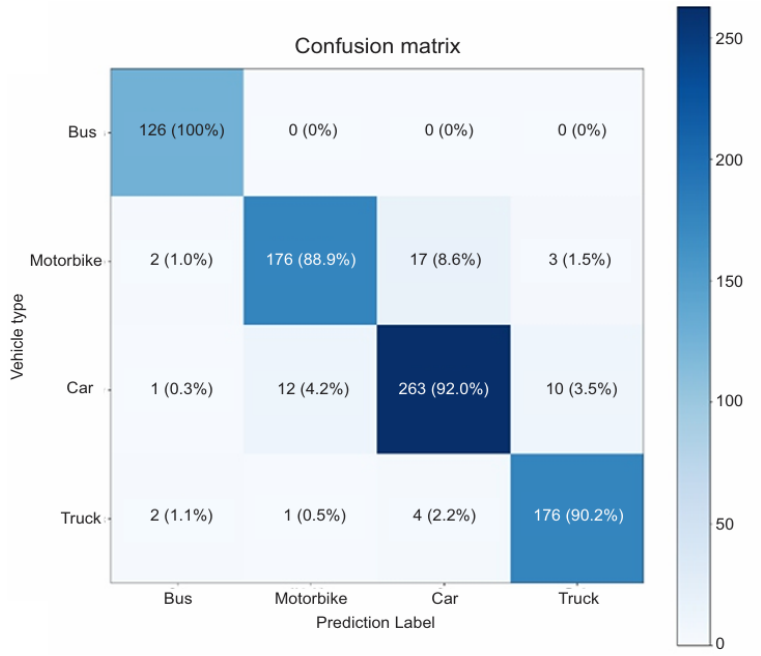

Fig. 9. Confusion matrix of the model trained and tested on PIR sensor and Lidar sensor

The AUC (Area Under the Curve) values for each class are: Bus: 1.00, Motorbike: 0.94, Car: 0.94, and Truck: 0.98, showing the high classification performance. The Micro-Average AUC is recorded at 0.96, while the Macro-Average AUC reaches 0.96, perform the model's stability across different vehicle types. However, the lower AUC values for the Motorbike and Car categories

are easier misclassification with Truck. Nevertheless, the performance gap between vehicle types is small, proving that the model still performs effectively in Fig. 10.

Table 1 provides a detailed classification performance for each vehicle category. The highest classification accuracy is achieved for the Bus (96.2% precision, 100% recall, and 98.0% F1-score), followed by Car with a Precision of 92.6%, Recall of 91.96%, and F1-score of 92.3%. On the other hand, the Motorbike and Truck categories exhibit lower accuracy, with Motorbike achieving a Precision of 93.1%, Recall of 88.9%, and F1-score of 90.9%, while Truck show a Precision of 93.1%, Recall of 96.2%, and F1-score of 94.6%. These results align with those shown in Table 1, where the Car and Truck categories tend to be confused with the Motorbike category.

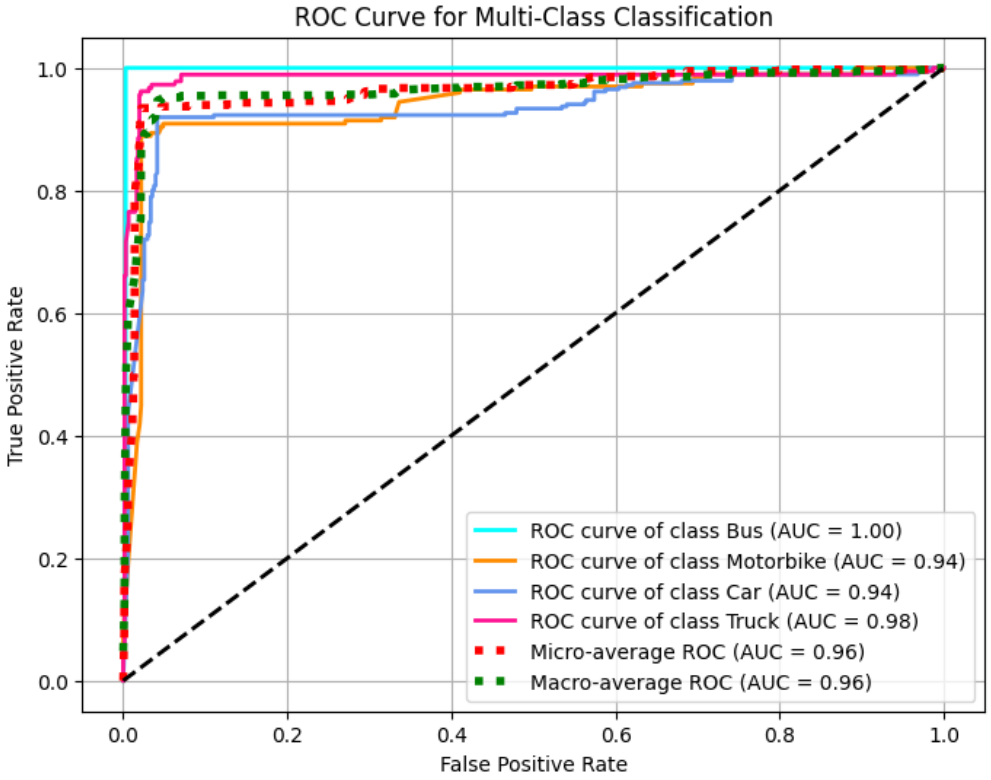

Fig. 10. ROC curve of the model trained and tested on PIR sensor and Lidar sensor

Table 1. model precision on each class

Class	Precision	Recall	F1-Score
Bus	96.2%	100%	98.0%
Motorbike	93.1%	88.9%	90.9%
Car	92.6%	91.96%	92.3%
Truck	93.1%	96.2%	94.6%

The study confirms that the LRF + PIR sensor fusion approach delivers high classification performance even in real-world traffic conditions. The model effectively distinguishes between different vehicle groups, especially Bus and Truck. However, some issue still remained in classifying Motorbike and Car due to the similarity in sensor signal characteristics. For improving performance, further dataset expansion, algorithm optimization, or the inclusion of additional features should be considered to minimize misclassification among vehicle types with special signals are approximately the same.

4. Conclusion

In this study, a real-time vehicle classification system based on the combination of Laser Rangefinder (LRF) and Pyroelectric Infrared (PIR) sensors was presented. Data acquisition was

performed over multiple months in real environments with an experiment roadside set up. The signals obtained from the two sensors were processed to show the geometric and thermodynamic features, which work well in the vehicle classification. Experimental results showed that our artificial neural network model achieved an average accuracy of 94%, with the minimum accuracy of 91% for each specific vehicle type. By combining information from the two types of sensors, the system can maintain stable accuracy even in low-light conditions or noisy environments. Using a neural network with two hidden layers helps balancing features extraction and computing efficiency, ensuring that the system can be deployed on embedded devices without requiring too much hardware resources. However, some challenges still exist, especially in bad weather conditions such as fog or heavy rain, where PIR sensors are easy affected by ambient temperature and LRF signals can be affected by unwanted factors. Therefore, the results show that the published model has high potential for application in intelligent transportation systems, especially in automatic vehicle monitoring and real-time utility vehicle classification. Furthermore, this approach can be extended to pedestrian recognition or traffic anomaly detection, supporting system warning and autonomous vehicle control. In the future, research will focus on improving the ability to control disturbances by applying advanced filtering algorithms, optimizing the model to develop declarations on low-performance microcontrollers, and expanding the dataset with many other environmental conditions to ensure the generality of the system.

The practical applications of this LRF-PIR fusion system extend beyond basic classification to enhance Intelligent Transportation Systems (ITS), including adaptive traffic signal control, automated tolling differentiated by vehicle class, and real-time incident detection in urban corridors such as Hanoi. Future expansions hold significant potential: incorporating additional modalities (e.g., acoustic sensors for engine noise) could mitigate weather-induced errors, while federated learning across networked nodes would scale the system for city-wide coverage. Moreover, adapting the MLP architecture for pedestrian or anomaly detection paves the way for safer autonomous driving ecosystems, aligning with global smart city initiatives.

Acknowledgement:

This research is funded by Hanoi University of Science and Technology (HUST) under project number T2024-TĐ-028.

References

[1]. J. Zhang, F.-Y. Wang, K. Wang, W.-H. Lin, X. Xu, C. Chen. (2011). Data-driven intelligent transportation systems: A survey. *IEEE Transactions on Intelligent Transportation Systems*, 12(4), 1624-1639. doi: 10.1109/TITS.2011.2158001

[2]. S. Kamkar, R. Safabakhsh. (2016). Vehicle detection, counting and classification in various conditions. *IET Intelligent Transport Systems*, 10(6), 406-413. https://doi.org/10.1049/iet-its.2015.0157

[3]. M. Al-Tarawneh, Y. Huang, P. Lu, D. Tolliver. (2018). Vehicle classification system using in-pavement fiber Bragg grating sensors. *IEEE Sensors Journal,* 18(7), 2807-2815. doi: 10.1109/JSEN.2018.2803618

[4]. , G. Dimitrakopoulos, P. Demestichas. (2010). Systems based on cognitive networking principles and management functionality. *IEEE Vehicular Technology Magazine,* 5(1), 77-84. DOI: 10.1109/MVT.2009.935537

[5]. Z. Sun, G. Bebis, R. Miller. (2004). On-road vehicle detection using optical sensors: A review. *Proceedings. The 7th International IEEE Conference on Intelligent Transportation Systems (IEEE Cat. No. 04TH8749)*, pp. 585-590. IEEE. doi: 10.1109/ITSC.2004.1398966

[6]. A. Gholamhosseinian, J. Seitz. (2021). Vehicle classification in intelligent transport systems: An overview, methods and software perspective. *IEEE Open Journal of Intelligent*

Transportation Systems, 2, 173-194. doi: 10.1109/OJITS.2021.3096756

[7]. , P. Sarcevic, S. Pletl, A. Odry. (2022). Real-time vehicle classification system using a single magnetometer. *Sensors*, 22(23), 9299. https://doi.org/10.3390/s22239299

[8]. E. Odat, J.S. Shamma, C. Claudel. (2018). Vehicle classification and speed estimation using combined passive infrared/ultrasonic sensors. *IEEE Transactions on Intelligent Transportation Systems*, 19(5) 1593-1606. doi: 10.1109/TITS.2017.2727224

[9]. , K. Lakshmanan, M. Roach, C. Giannetti, S. Bhoite, D. George, T. Mortensen, M. Manduhu, B. Heravi, S. Kariyawasam, X. Xie. (2023). A robust vehicle detection model for LiDAR sensor using simulation data and transfer learning methods. *AI*, 4(2), 461-481. https://doi.org/10.3390/ai4020025

[10]. J.D. Choi, M.Y. Kim. (2023). A sensor fusion system with thermal infrared camera and LiDAR for autonomous vehicles and deep learning based object detection. *ICT Express,* 9(2), 222-227. https://doi.org/10.1016/j.icte.2021.12.016

[11]. Z. Wang, J. Zhan, C. Duan, X. Guan, P. Lu, K. Yang. (2023). A review of vehicle detection techniques for intelligent vehicles. *IEEE Transactions on Neural Networks and Learning Systems*, 34(8), 3811-3831. doi: 10.1109/TNNLS.2021.3128968

[12]. GARMIN. Datasheet of PIR sensor Garmin LIDAR-Lite v3HP. https://www.garmin.com/en-US/p/578152#specs (accessed 08/09/2025)

[13]. Murata Manufacturing Co., Ltd. (2022). Datasheet of LRF sensor IRA-S200ST01A01. https://www.mouser.com/datasheet/2/281/1/IRA_S200ST01A01-2079850.pdf

[14]. KUBE Electronics AG. Datasheet of Fresnel Lens KUBE TR1007. https://www.kube.ch/home.htm#Docs (accessed 10/09/2025)

[15]. A. Tashakkori, M. Talebzadeh, F. Salboukh, L. Deshmukh, H. Talebzadeh. (2024). Forecasting gold prices with MLP neural networks: A machine learning approach. *International Journal of Science and Engineering Applications (IJSEA)*, 13(8), 13-20. DOI: 10.7753/IJSEA1308.1003

[16]. Y. Qu, H. Cai, K. Ren, W. Zhang, Y. Yu, Y. Wen, J. Wang. (2016). Product-based neural networks for user response prediction. *2016 IEEE 16th International Conference on Data Mining (ICDM), pp. 1149-1154. IEEE*. doi: 10.1109/ICDM.2016.0151.

[17]. Z. Shen, H. Yang, S. Zhang. (2020). Deep network approximation characterized by number of neurons. *Communications in Computational Physics*, 28(5), 1768-1811. https://doi.org/10.4208/cicp.OA-2020-0149

[18]. G. Lin, W. Shen. (2018). Research on convolutional neural network based on improved Relu piecewise activation function. *Procedia Computer Science*, 131, 977-984. https://doi.org/10.1016/j.procs.2018.04.239

[19]. S. Muruganandam, R. Joshi, P. Suresh, N. Balakrishna, K.H. Kishore, S.V. Manikanthan. (2023). A deep learning based feed forward artificial neural network to predict the K-barriers for intrusion detection using a wireless sensor network. *Measurement: Sensors,* 25, 100613. https://doi.org/10.1016/j.measen.2022.100613